






## Article

# Characteristics and Drivers of Marine Heatwaves in 2021 Summer in East Korea Bay, Japan/East Sea

Sijie Chen <sup>1</sup>, Yulong Yao <sup>2,3</sup>, Yuting Feng <sup>1,4,5</sup>, Yongchui Zhang <sup>6</sup>, Changshui Xia <sup>7,8</sup>,  
Kenny T. C. Lim Kam Sian <sup>9</sup> and Changming Dong <sup>1,2,3,\*</sup>

- <sup>1</sup> School of Marine Sciences, Nanjing University of Information Science & Technology, Nanjing 210044, China
- <sup>2</sup> Southern Laboratory of Ocean Science and Engineering (Guangdong Zhuhai), Zhuhai 519082, China
- <sup>3</sup> State Key Laboratory of Tropical Oceanography, South China Sea Institute of Oceanography, Chinese Academy of Sciences, Guangzhou 510301, China
- <sup>4</sup> Faculty of Chemistry and Environment Science, Guangdong Ocean University, Zhanjiang 524088, China
- <sup>5</sup> Research Center for Coastal Environmental Protection and Ecological Remediation, Guangdong Ocean University, Zhanjiang 524088, China
- <sup>6</sup> College of Meteorology and Oceanography, National University of Defense Technology, Nanjing 211101, China
- <sup>7</sup> First Institute of Oceanography, Ministry of Natural Resources, Qingdao 266061, China
- <sup>8</sup> Laboratory for Regional Oceanography and Numerical Modeling, Pilot National Laboratory for Marine Science and Technology (Qingdao), Qingdao 266237, China
- <sup>9</sup> School of Atmospheric Science and Remote Sensing, Wuxi University, Wuxi 214105, China
- \* Correspondence: cmdong@nuist.edu.cn; Tel.: +86-025-58695733

**Abstract:** Marine heatwaves (MHWs) are persistent, discrete, extreme high-temperature events in the ocean, which can destructively affect marine ecosystems. Using satellite remote sensing data and reanalysis data from 1982 to 2021, we find that six indices characterizing the MHWs are in a remarkable increasing trend in the Japan/East Sea (JES), which shows that the most severe MHW events take place in the East Korean Bay (EKB) in the summer of 2021. Based on this finding, the present study focuses on the characteristics and mechanisms of the MHWs in the EKB and its adjacent areas from June to August 2021. The analysis reveals that the total days and mean intensity of MHWs that occur in the EKB are 1.84 and 1.47 times more than those averaged in the JES, respectively. It is shown that mechanisms for the occurrences of the MHWs in the summer of 2021 are caused by the atmospheric high-pressure system moving to the EKB area. Other reasons also decrease the water cooling: the net positive lateral heat fluxes across open boundaries, and the weak sea surface wind over the EKB area. Other possible reasons which cause the summer MHW events in 2021 need the oceanic numerical models to further investigate the issue.

**Keywords:** marine heatwaves; heat flux; sea surface temperature; East Korea Bay; long-term trends



**Citation:** Chen, S.; Yao, Y.; Feng, Y.; Zhang, Y.; Xia, C.; Sian, K.T.L.K.; Dong, C. Characteristics and Drivers of Marine Heatwaves in 2021 Summer in East Korea Bay, Japan/East Sea. *Remote Sens.* **2023**, *15*, 713. <https://doi.org/10.3390/rs15030713>

Academic Editor: Jorge Vazquez

Received: 30 November 2022

Revised: 4 January 2023

Accepted: 19 January 2023

Published: 25 January 2023



**Copyright:** © 2023 by the authors. Licensee MDPI, Basel, Switzerland. This article is an open access article distributed under the terms and conditions of the Creative Commons Attribution (CC BY) license (<https://creativecommons.org/licenses/by/4.0/>).

## 1. Introduction

The ocean has a large specific heat capacity and absorbs more than 90% of heat due to global warming; the ocean has significantly warmed in recent years, especially the upper ocean (0–700 m) [1,2]. Compared to the pre-industrial revolution era (1850–1900), the sea surface temperature (SST) in 2011–2020 has increased by 0.88 °C (0.68–1.01 °C), of which 0.60 °C (0.44–0.74 °C) occurred after 1980 [3]. Such global warming trend could lead to local anomalous warm events, such as marine heatwaves (MHWs), which were defined first by Pearce et al., (2011) [4]. The detailed quantitative definition of MHWs can be found in Section 2.2.1. MHWs can last days to months, covering several to thousands of square kilometers [5]. According to statistical analysis of observational data, from 1925 to 2016, the global average duration, frequency, and total number of MHWs increased by 17, 34, and 54%, respectively [6]. MHWs can destructively affect marine ecosystems, such as leading to substantial coral reef bleaching and significant reductions in kelp forests and seagrass beds [7,8]. Under the background of global warming, MHWs are projected to occur more

frequently and be sustained for longer. Even annual continuous MHWs are expected at the end of this century [9,10].

MHWs are caused by a combination of local atmospheric and oceanic processes and may be modulated by large-scale climate variability, including teleconnections [11]. A strong atmospheric high-pressure system over the ocean is accompanied by lower cloud coverage, which could lead to enhanced solar radiation, resulting in more heat transport into the ocean. The weaker sea surface wind could cause weaker vertical mixing in the upper ocean and keep more heat at the sea surface [11–13]. Moreover, more horizontal and vertical heat advection by oceanic currents, such as coastal upwelling or Ekman pumping, also can cause an increase in local SST [11,14,15]. All the above local physical processes could result in the occurrence of MHWs.

The previous studies indicated that the northwestern Pacific was one of the most serious oceanic regions where MHWs took place in the last half a century [6,16–18]. As a semi-closed marginal sea in this area, the Japan/East Sea (JES) witnesses the frequent occurrences of MHWs, as suggested by a recent study [19]. Since the JES is surrounded by four countries, including North Korea, South Korea, Russia, and Japan, a high density of the population is affected when the MHWs take place. The JES carries an abundance of plankton and aquatic resources, which could be severely influenced by the MHWs. Therefore, further study of the JES MHWs is needed.

The JES is connected with the open ocean through four channels: Korea Strait (also called Tsushima Strait) connecting the Yellow Sea, Tatarsky Strait connecting the Sea of Okhotsk, Tsugaru Strait and Soya Strait connecting the northern Pacific, see Figure 1. Figure 1 illustrates that the only cold current entering the JES is the Liman Current from the Sea of Okhotsk through the Tatarsky Strait, while the warm water is a branch of the Kuroshio Water with high temperature and salinity flowing from the Korea Strait. The current from the Korea Strait runs along the west boundary to the East Korean Bay (EKB) to the north, which forms a strong sea surface anticyclonic circulation [20]. A subpolar front forms at 40°N in the JES due to the intersection of cold and warm currents.

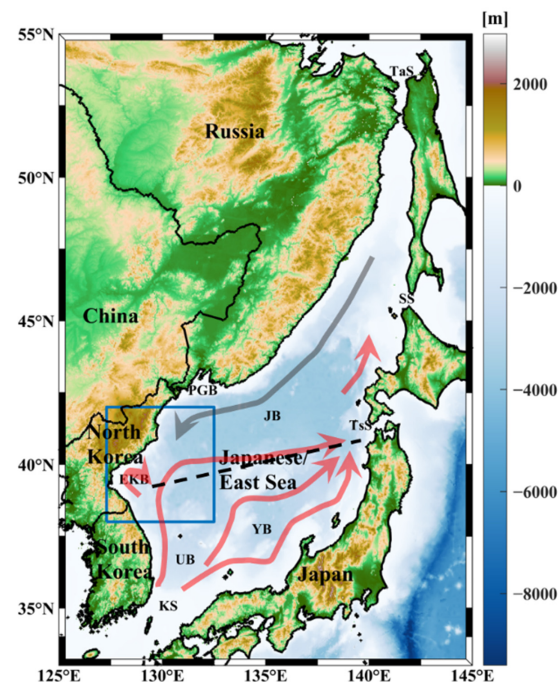


**Figure 1.** The topography (background color) in the study area and sea surface current schematic figure (arrows). The blue box is the extended EKB area (127.3°E–132.5°E, 38°N–42°N), and the black dotted line is the subpolar front. The red arrows indicate warm currents, while the gray arrows indicate cold currents. EKB: East Korean Bay; JB: Japan Basin; UB: Ulleung Basin; YB: Yamato Basin; PGB: Peter the Great Bay; KS: Korea Strait (Tsushima Strait); SS: Soya Strait; TaS: Tatarsky Strait; TsS: Tsugaru Strait.

It is found that the JES is one of the sea areas with the highest warming rate of SST ( $0.45^{\circ}\text{C}$ ) in the coastal areas of the northwestern Pacific, especially in summer [21]. From July to August 2021, strong MHW events are presented in vast areas of the northwestern Pacific, including the JES, which are at maximum intensity since 1982 [17]. Wang et al. (2022) analyze 1982–2020 satellite remote sensing SST data and point out that frequent MHWs are observed in the JES in August, and the annual average sum of MHWs intensity has increased sharply in the JES, more than twice the global average trend [19]. It is seen that the EKB is the area where the most severe MHWs take place in the JES.

To better understand the MHWs in the EKB, the present study mainly focuses on the summer MHW events in the EKB and adjacent sea areas in 2021. In the rest of the paper, Section 2 is Data and Methods, describing the data and methods used in the present study; Section 3 is Results, in which the analytical results of the data are presented, followed by Discussion and Conclusions in Sections 4 and 5, respectively.

## 2. Data and Methods

### 2.1. Data

#### 2.1.1. Observational Satellite Remote Sensing Data

Daily satellite SST data used for the present study are from the High-Resolution Dataset Version 2 of the National Oceanic and Atmospheric Administration (NOAA) Optimum Interpolation Sea Surface Temperature (OISST) [22] with a spatial resolution of  $0.25^{\circ}$ , covering the period from 1982 to 2021. The coarse long-term SST data are used for identifying the MHW events. The daily satellite SST data obtained from the Group for High-Resolution Sea Surface Temperature (GHRSSST) with a resolution of 9 km are used for the detailed features of MHW events (since the high-resolution SST data are available only for a shorter period from 2002–2021). The study area EKB is the one covering  $127.3^{\circ}\text{E}$ – $132.5^{\circ}\text{E}$ ,  $38^{\circ}\text{N}$ – $42^{\circ}\text{N}$ .

Daily sea level anomaly (SLA) computed with a 20-year mean reference period (1993–2012), and sea surface geostrophic velocity anomaly are used from Archiving, Validation, and Interpretation of Satellite Oceanographic (abbreviation as AVISO) with a spatial resolution of  $1/4^{\circ}$ , which can be used in mesoscale eddies detection [23,24].

Chlorophyll (CHL) data are used from the Globcolour database, which is an 8-day mean product of multi-satellite merged data on a spatial grid of 4 km from 1997 to 2021.

#### 2.1.2. Reanalysis Data

To investigate the characteristics of atmospheric and oceanic circulation during MHWs, several variables are analyzed in this study from June to August 2021: total surface net solar radiation, surface net thermal radiation, surface latent heat flux, surface sensible heat flux, geopotential height data at 500 hPa, and 10-m wind speed are from the fifth-generation global atmospheric reanalysis data (abbreviation as ERA5) and from the European Centre for Medium-Range Weather Forecasts (abbreviation as ECMWF). The variables used from the ERA5 are monthly means with a horizontal resolution of  $1/4^{\circ}$  from 1979 to 2021.

### 2.2. Methods

#### 2.2.1. Definition of Marine Heatwaves

The definition of a MHW provided by Hobday et al. [5] is a prolonged warm-water event whose duration is at least 5 days and the threshold is a 90th percentile above the perennial climatological SST. The gap between the two events must be at least 2 days. The climatological threshold with the seasonal change is calculated from the data within an 11-day window centered on each day within the climatological period and then smoothed using a 31-day moving average. The climatological means and seasonal means are based on the 1982–2021 OISST data. This definition is also used in previous studies on MHWs in the JES [17,19].

Following previous studies [5,6,25], six indices are used to represent MHW characteristics, including the number of MHWs per year (Frequency, unit: Counts), the total

days of MHWs per year (Days, unit: Days), average MHW duration of MHWs per year (Duration, unit: days/count), the maximum intensity of MHWs per year (MaxInt, unit: °C/count, intensity means SST minus the corresponding threshold during an MHW event), the average intensity of MHWs per year (MeanInt, unit: °C/count), and multiply the accumulation of average duration (CumInt, unit: °C).

In this study, we use the MATLAB main function code developed by Zhao and Martin [26] ([https://github.com/ZijieZhaoMMHW/m\\_mhw1.0](https://github.com/ZijieZhaoMMHW/m_mhw1.0), accessed on 24 January 2019) to detect MHWs. In addition, this study also uses linear trend analysis and the Mann–Kendall test [27].

### 2.2.2. Area-Weighted

The data used are gridded data. The value on each grid represents the rectangular area next to the grid. In the spheric coordinate by latitude-longitude, the area around one grid varies with latitude:

$$S = \frac{2\pi R_p \times \alpha^\circ}{360^\circ} \times \frac{2\pi R_E \times \cos \phi \times \alpha^\circ}{360^\circ}, \quad (1)$$

$S$  is the area calculation,  $R$  is the earth radius,  $\alpha^\circ$  is the data spatial resolution.

### 2.2.3. Oceanic Heat Flux across Boundaries of the Study Area

In the upper ocean, the SST variation is controlled by heat fluxes across its lateral boundaries, sea surface, and bottom boundary. The study area EKB includes three open lateral boundaries: southern, northern, and eastern, see the blue box in Figure 1. The heat fluxes across the southern and northern boundaries are calculated by the following formula:

$$F_{S/N} = \int_{x_1}^{x_2} \int_{-D}^0 \rho C_P T \vec{V} dz dx \quad (2)$$

The heat flux across the eastern boundary is calculated by the following formula:

$$F_E = \int_{y_1}^{y_2} \int_{-D}^0 \rho C_P T \vec{U} dz dy \quad (3)$$

The lateral total heat flux is calculated by the following formula:

$$F_{LT} = F_S - F_N - F_E, \quad (4)$$

where  $F_{S/N}$  is the heat flux across the southern (northern) boundary,  $F_E$  is the heat flux across the eastern boundary,  $F_{LT}$  is the total lateral heat flux.  $x_1$  and  $x_2$  are 128.6°E and 132.5°E, respectively, at the latitude of 38°N (42°N) for the southern (northern) boundary.  $y_1$  and  $y_2$  of the eastern boundary are 38°N and 42°N, respectively, at the longitude of 132.5°E.  $D$  is the depth to calculate the seawater heat flux and is set as 10 m for the summer [28], where the seawater temperature is assumed to be the same as SST.  $\rho$  is the mean seawater density (1025 kg/m<sup>3</sup>), and  $C_P$  is seawater heat capacity (3986 J kg<sup>-1</sup>K<sup>-1</sup>) and  $T$  is SST.  $U$  and  $V$  are the eastward and northward velocities, respectively. Formula (3) implies that the positive (negative) values of  $F_{LT}$  represent the heat flux into (out of) the study area.

## 3. Results

### 3.1. 1982–2021. MHWs Statistical Analysis

To better understand how severe the summer MHW events are in the JES, we conduct a comprehensive statistical analysis of the OISST data in this area from 1982 to 2021. Figure 2 shows the multi-year average metrics of MHWs in the JES for 40 years: total days, frequency, duration, maximum intensity (MaxInt), mean intensity (MeanInt), and cumulative intensity (CumInt). It is demonstrated that there have been MHWs taking place in the JES in the last 40 years and more and stronger MHWs are found in the EKB area.

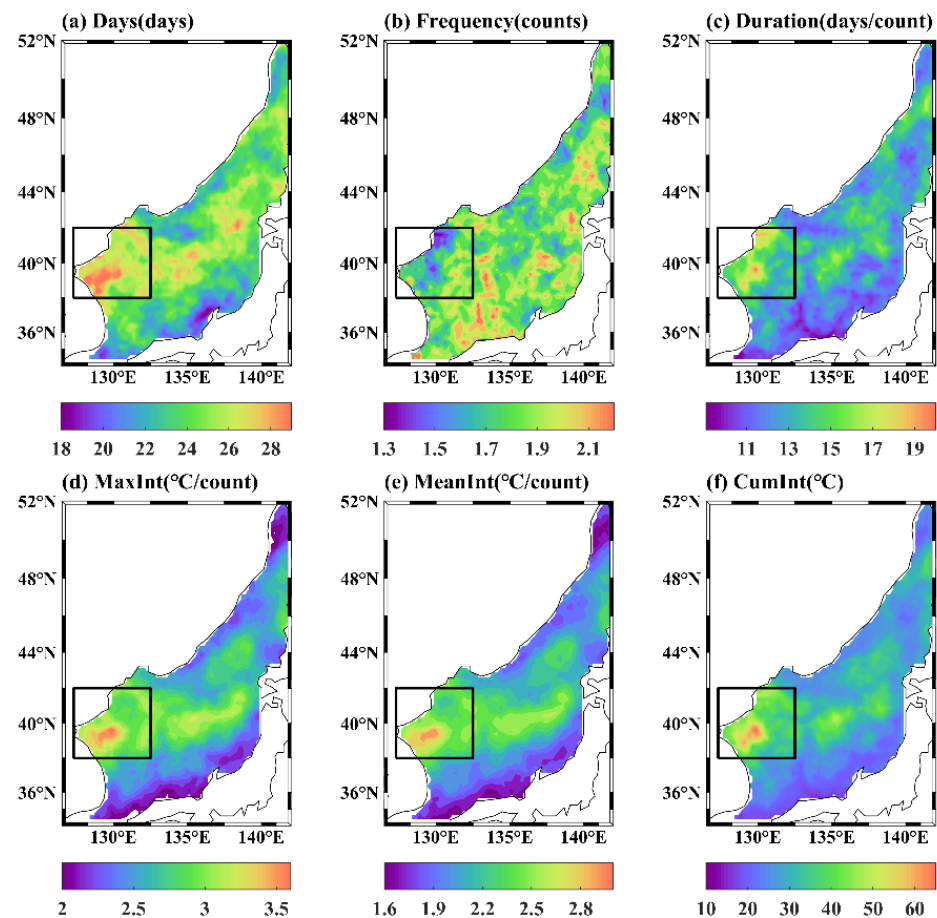


**Figure 2.** Spatial distributions of 40-year average during 1982–2021 all year: (a) total MHW days, (b) frequency, (c) duration, (d) MaxInt, (e) MeanInt, and (f) CumInt in the JES. The black box indicates the study area.

Figure 2a shows that more total days are observed in the central of the JES, compared to the northern and southern coastal regions, with the highest number of 25–29 days in the EKB area, 23–28 days in the JB, and fewer than 22 days in the rest of the JES. Figure 2b indicates that the frequency of MHW occurrences can reach more than 1.9 counts/year in the southern JES, showing a discontinuous band distribution. An average of 1.6–1.9 counts/year occurs in most of the southern region, compared with the low frequency (less than 1.6 counts/year) in the northern and eastern regions. The distribution of the MeanInt in Figure 2c is similar to Figure 2a, with high-value regions mainly in bands in the EKB area (14–20 days/count) and central (13–16 days/count) of the JES, and less than 13 days/count in other areas. The spatial distribution patterns of MaxInt, MeanInt, and CumInt are nearly identical, shown in Figure 2d–f. The strongest intensity areas of MHWs are found in the EKB area. For example, in the EKB areas, the MaxInt reaches 3–3.7 °C/count, and the MeanInt reaches 2.5–3 °C/count, while CumInt is 45–65 °C. In the central JES, they reach 2.5–3 °C/count, 2–2.5 °C/count and 30–45 °C, respectively, followed by MaxInt (less than 2.5 °C/count), MeanInt (less than 2 °C/count) and CumInt (less than 30 °C) along the northern and southern coasts (Figure 2d–f).

Similar results are obtained by Wang et al. [19] using 39-year data (1982–2020). Based on Figure 4 from Wang et al. (2022) and Figure 2, one can see clearly that large values in the EKB out of the JES for five of six indices: Days, Duration, and three intensity indices, which causes severe damage to the ecological system. Only a small number is for Frequency, which does not affect environments if the intensity is low. These inspire us to focus our attention on the EKB for the study of the MHWs in the JES. It can be seen clearly that high values are presented in the EKB area with five out of six indices that characterize



the features of the MHW, especially including the variables for the intensity and duration causing severe damage to the ecological system. The only value in the EKB is frequency, which has a low impact on the environment. Therefore, when one studies the MHWs in the JES, the focus should be put on the EKB, which justifies our selection for the study area for the present MHW study as the EKB. Therefore, MHW events in this area are more likely to persist for long-term events, which could have severe impacts on the coastal population and marine ecology.

Figure 3 exhibits consistently and rapidly increasing trends in all area-weighted average indices ( $p < 0.01$ ), reaching the highest values in 2020 and 2021. The increasing rates of Days and CumInt are most pronounced, which are  $1.04 \pm 1.46$  days/10a and  $1.10 \pm 1.79$  °C/10a, respectively; 40-year Days in Figure 3a are high in 2008, 2017, 2019, 2020, and 2021, with a correlation coefficient of 0.80. The Days in 2021 even reached 88 days/year and in four other years nearly 50 days/year. The growth rates of Frequency and Duration are  $0.53 \pm 0.11$  counts/10a and  $0.23 \pm 0.45$  days/count/10a, respectively. The Frequency is more than three counts in 2008, 2017, and 2021, compared to less than two counts before 2008, and the highest frequency is in 2021 (3.5 counts), with a correlation coefficient of 0.87 (Figure 3b). The low Duration is less than 15 days before 2019, while it changes significantly in 2020 (29 days) and 2021 (18 days), with a correlation coefficient of 0.90, see Figure 3c. MaxInt and MeanInt demonstrate slight increasing trends at  $0.02 \pm 0.05$  °C/count/10a and  $0.01 \pm 0.04$  °C/count/10a (Figure 3d,e), respectively. The MaxInt (MeanInt) is also high in 2018, 2020, and 2021, at approximately 2.8 °C/count (2.2 °C/count), with the correlation coefficient of MaxInt (MeanInt) 0.91 (0.47) (Figure 3d,e). The time series of CumInt is similar to the Duration, which is less than 50 °C before 2019 and exceeds 140 °C and 80 °C in 2020 and 2021, respectively, with a correlation coefficient of 0.86 (Figure 3f).

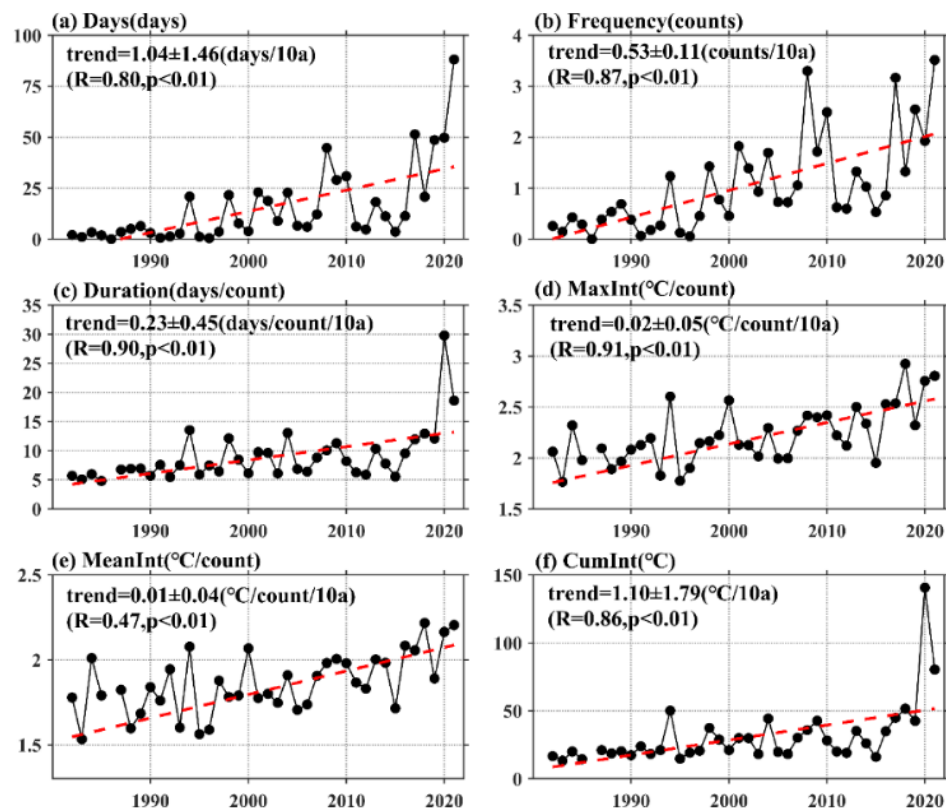


**Figure 3.** Temporal evolution distributions of area-weighted average (a) total MHW days, (b) frequency, (c) duration, (d) MaxInt, (e) MeanInt, and (f) CumInt in the EKB during 1982–2021 all year. The red dotted lines are linear trends, and the  $p$ -value significance level is calculated using the Mann–Kendall trend test.

Values presented in Table 1 for the MHW indices of high numbers in the EKB area are extracted from Figure 3, in which the indices in 2008, 2017, 2018, 2019, 2020 and 2021 are chosen. It can be seen obviously that the year of 2021 witnesses the highest numbers of Days (90.14 days), Frequency (4.67 counts), MaxInt (2.34 °C/count) and MeanInt (1.85 °C/count) in 40 years in the EKB. The Duration and CumInt of 2021 ranked second among all years (14.84 days/count and 41.32 °C, respectively), and are much higher than those in the previous 38 years. Therefore, severe MHWs in the JES in 2021 need further investigation.

**Table 1.** MHWs indices in high numbers.

Index	Unit	2008	2017	2018	2019	2020	2021
Days	Days	29.16	33.11	23.02	46.28	55.03	90.14
Frequency	Counts	2.66	2.70	1.81	3.34	2.92	4.67
Duration	Days/count	7.87	8.32	10.36	9.07	16.84	14.84
MaxInt	°C/count	2.11	2.03	2.30	1.95	2.10	2.34
MeanInt	°C/count	1.72	1.70	1.85	1.60	1.68	1.85
CumInt	°C	18.78	20.00	27.16	20.20	48.11	41.32

### 3.2. Analysis of MHW Events in the EKB in the Summer of 2021

Based on the above analysis of Figures 2 and 3 and previous research on intense MHWs in the summer of 2021 [17], in this section, we examine in detail the MHW events in the EKB in the summer of 2021.

Figure 4 shows the spatial distributions of the six indices for MHWs in the study areas from June 1st to August 31st, 2021. It can be seen clearly that the six indices are very high in the study area (marked by the black rectangle).

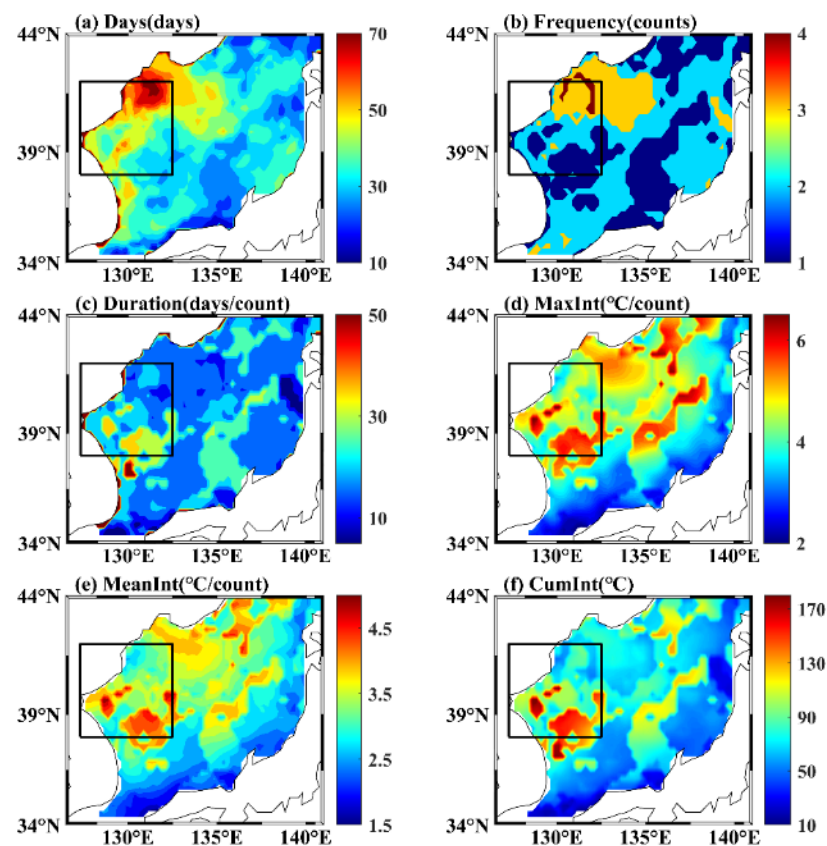


**Figure 4.** Same as Figure 2, but for 1 June to 31 August 2021.

From Figure 4a,b, one can see that the total number of days and frequency in the northern area is higher in the study area. Shown in Figure 4a, a high Days spot (50–70 days) can be observed in the northern part of the EKB, and a similar distribution pattern can be found in Frequency shown in Figure 4b with four counts in the northern part of the EKB and one to two counts in most other areas. In Figure 4c, durations of 20–35 days/count are found in the south of the EKB area. The distribution patterns of MaxInt, MeanInt and CumInt in Figure 4d–f are nearly identical. In the EKB, strong-intensity areas are found around the location (39.5°N, 129°E), up to 6.5 °C of MaxInt, followed by 6–6.5 °C in the southern of the EKB area (Figure 4d). In Figure 4e, however, MeanInt reaches more than 4.5 °C in the central and southern of the EKB area and others are less than 3.5 °C. The CumInt is more pronounced in the central and southern of the EKB area, up to 150–170 °C, than in other areas with no more than 120 °C (Figure 4f).

To further examine MHWs in the summer of 2021, using high-resolution SST data GHRSSST, we analyze the monthly average SST anomalies and choose a specific single point to plot the daily SST time series with the MHW event criteria from June to August 2021 (Figure 5). It can be seen clearly that the SST anomalies in July are the most significant, and those in the EKB area are also high in June and August.

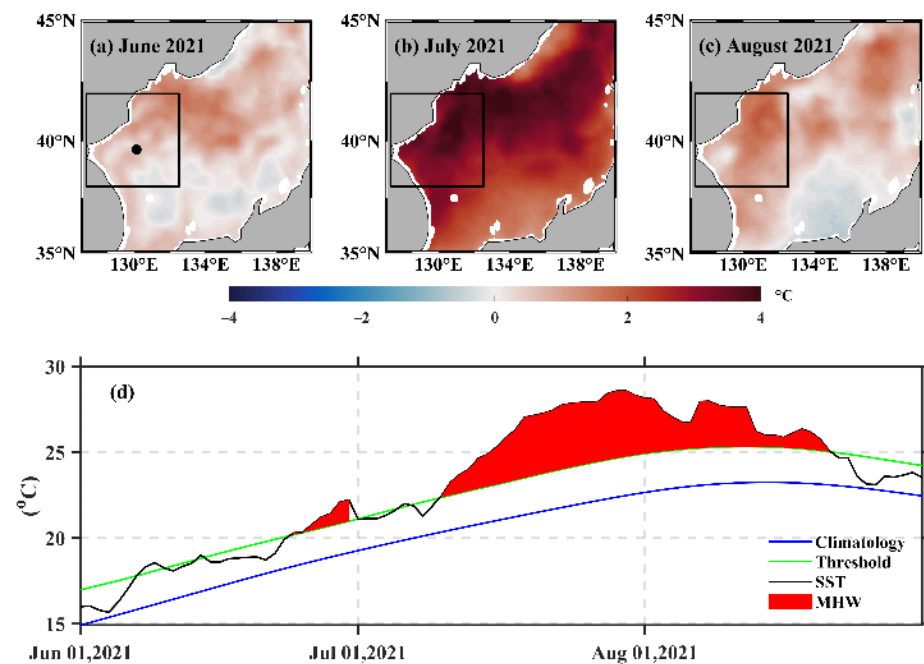


**Figure 5.** (a–c) SST anomalies from June to August 2021 (units: °C). The black box is the study area. (d) Event line for detected MHWs at the black dot in (a). The blue, green, and black curves are the climatology, the 90th percentile threshold, and SST, respectively. The red-shaded regions indicate MHW events.

In Figure 5a, the SST anomaly located between PGB and its adjacent area is positive with a maximum of 2 °C, followed by the positive SST anomaly in most of the EKB area. In Figure 5b, the positive SST anomaly in July covers almost the whole region, especially at the EKB-PGB area (up to 4 °C). In Figure 5c, the highest positive SST anomaly is also found in the EKB in August, which is approximately 2 °C. Figure 5d is the event line for detected MHWs at the black dot (130.125 °E, 39.625 °N) in Figure 5a. The result shows a continuous high-intensity MHW event from July 10 to August 21, with the highest SST reaching 28 °C, which is 5 °C higher than the climatological SST of the same period from 1982 to 2021.

In summary, based on the above analysis, it is demonstrated that severe MHW events in the EKB take place in the summer of 2021. The reasons causing the events are discussed in Section 3.3.



### 3.3. Driving Mechanisms for MHW Events in the EKB in the Summer of 2021

In terms of the heat balance, the local SST increase could be caused by the heat fluxes in open boundaries including the lateral, top, and bottom of a study area. In this section, we analyze the driving mechanisms behind the MHW events in the EKB in summer 2021 from both atmospheric and oceanic perspectives: vertical heat flux at the sea surface, lateral heat flux from open boundaries, and effects of vertical mixing.

#### 3.3.1. Vertical Heat Flux at the Sea Surface

The atmospheric circulation at mid-latitudes may affect the local net heat fluxes at the air-sea interface, thus impacting SST and resulting in an MHW event [7,12,13,29,30]. The high-pressure system over East Asia in the summer of 2021 is stronger compared with the same period in normal years. The western Pacific subtropical high (WPSH) strengthens and expands, and its ridge line extends further west and north [17]. The 500 hPa geopotential height over the JES shows a positive anomaly [31].

In Figure 6a–c, we plot the spatial distributions of 500 hPa geopotential heights in June, July, and August 2021, respectively. It can be seen that the high-pressure ridge over the JES, including the EKB area, forms in July and moves northward between July and August (Figure 6a–c). In Figure 6d–e, anomalies of 500 hPa geopotential heights relative to the 40-year mean (1982–2021) are plotted. In June 2021 when the high pressure has not yet formed, a negative pressure anomaly exists in the west of the JES, northeastern China (−10 gpm, Figure 6d). In July, a high-pressure center is observed in the northern JES with a maximum positive anomaly of 90 gpm, and the periphery of the high-pressure system has an impact on the EKB area (Figure 6e). In August, the center moves northward to the Okhotsk Sea and weakens to 80 gpm. At the same time, a low-pressure system appears and is larger and stronger in the western JES (−20 gpm, Figure 6f).

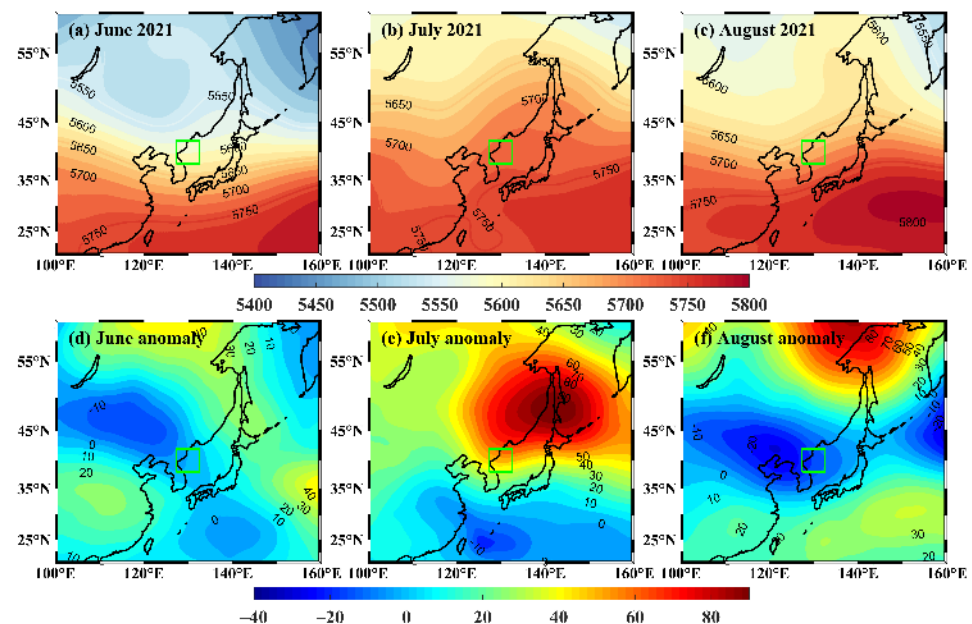


**Figure 6.** 500 hPa geopotential heights (units: gpm), (a–c) Blocking high from June to August 2021, (d–f) Geopotential height anomalies from June to August 2021, relative to the climatology (1982–2021). The green box is the study area.

It can be seen that among the four heat fluxes, the net shortwave radiation and the net latent radiation are the largest, with a maximum (minimum) of  $240 \text{ W/m}^2$  ( $-80 \text{ W/m}^2$ ) in the studied area (Figure 7a–c and 7g–i). June and July witness high net shortwave radiation, which drops in August (Figure 7a–c). The net latent radiation shows the opposite trend. It reaches its minimum value in August, which can be explained by warmer water in August

increasing the release of latent heat into the atmosphere [27] (Figure 7g–i). In contrast, the net surface longwave heat flux and the net surface sensible heat flux are much smaller. The total net heat fluxes in June and July are about  $150 \text{ W/m}^2$  while decreasing to  $-50 \text{ W/m}^2$  in August (Figure 7m–o). As a result, the heat flux at the sea surface is the highest in the EKB area in July, providing a condition of high SST.

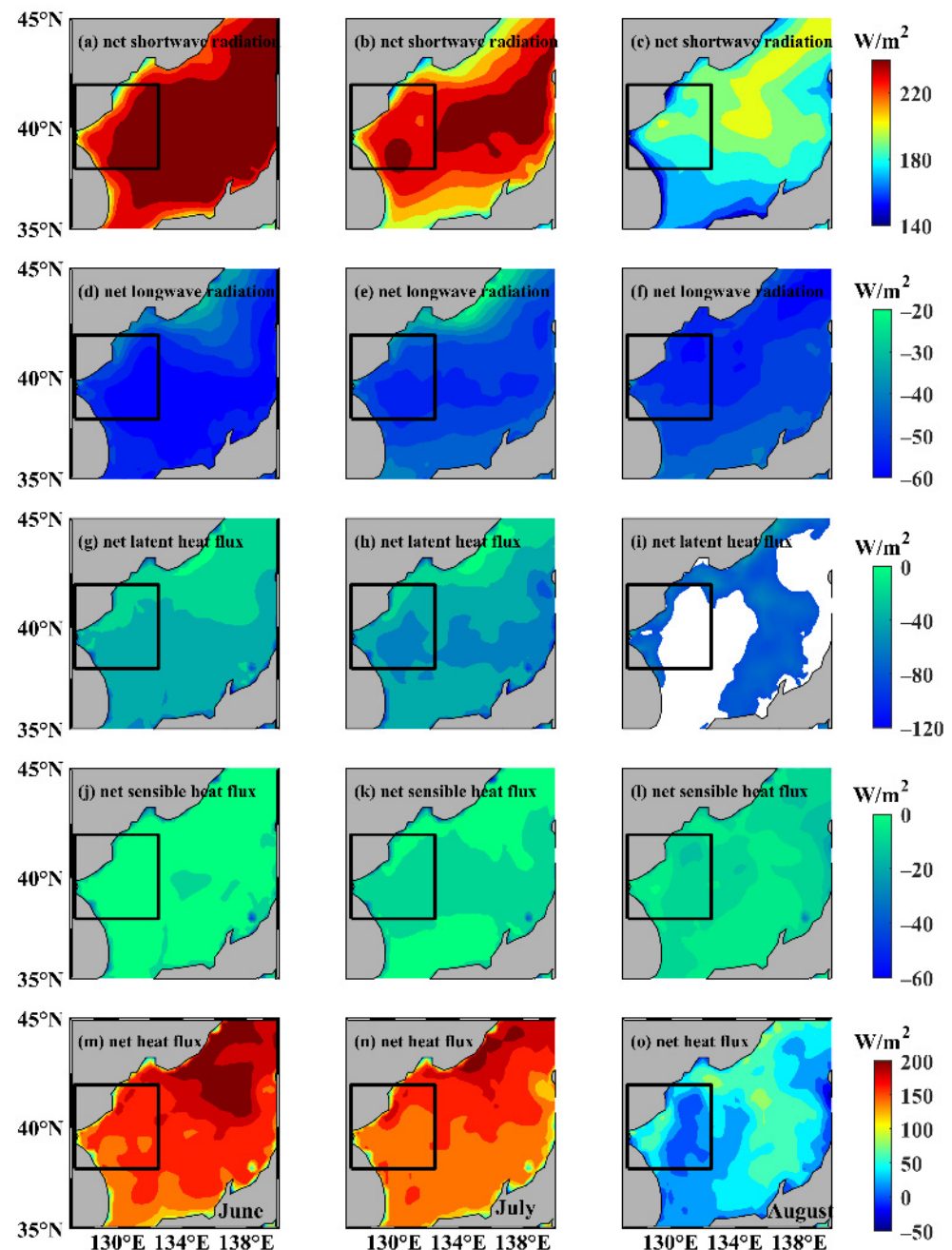


**Figure 7.** Spatial distribution of (a–c) net shortwave radiation, (d–f) net longwave radiation, (g–i) net surface latent heat flux, (j–l) net surface sensible heat flux, (m–o) net surface heat flux (units:  $\text{W/m}^2$ , all fluxes are positive downward) from June to August 2021.

### 3.3.2. Lateral Heat Fluxes from Open Boundaries

According to previous studies, the warm current transport from the Korea Strait shows an increasing trend in all months from 1989 to 2018, especially in the spring and summer [32]. We have discussed the analysis of the heat flux across the sea surface in Section 3.3.1, and in this section, lateral heat fluxes across open boundaries are explored.

In Figure 8, we calculate the heat fluxes across the boundaries using Formula (1–3). In Figure 8a, the heat flux across the eastern boundary is the highest (approximately 1–2 GW), followed by the southern boundary (at about 1 GW), both increasing in the middle of June and late July. Since high-intensity areas are mainly near the southern boundary (Figure 4d–f), heat fluxes across the southern boundary could be one of the reasons that maintain the stronger intensity of MHWs. It can be seen that the zonal heat flux is more than the meridional ones. The heat flux across the northern boundary is the smallest (usually negative), and there is a negative peak in early August. From the total heat flux for the three boundaries, it can be found that there is less heat loss during 18–27 June (AB) and 20 July–11 August (CD). The total heat flux is greater than 0 on 6–13 August, resulting in heat accumulation in the EKB area (red-shaded area, less than 0.2 GW) (Figure 8b). Hence, lateral heat flux, mainly in late July and early August, maintains a high SST.

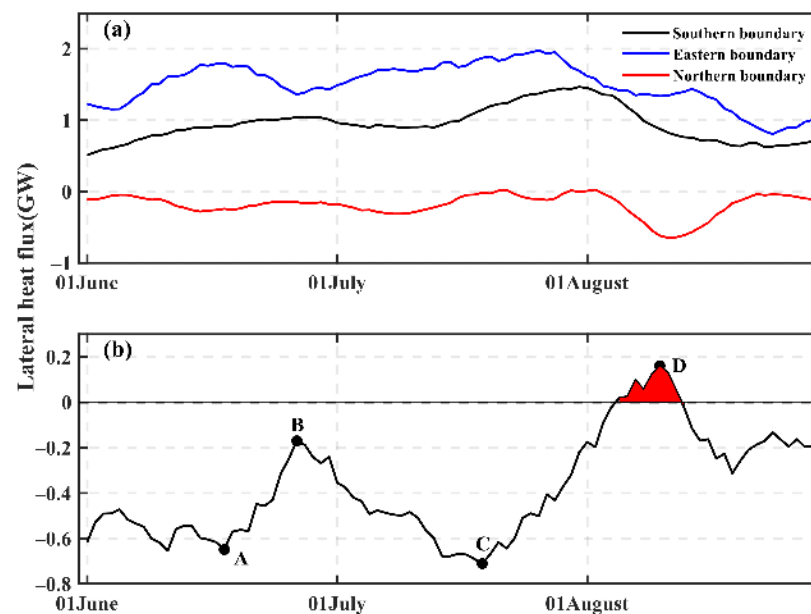


**Figure 8.** Lateral heat fluxes from June to August 2021 (unit: GW). (a) Heat fluxes across the northern (red line), southern (black line), and eastern boundaries (blue line). (b) Total heat flux across the three boundaries, with positive values representing regional heat accumulation (red-shaded area). The four points A, B, C, and D in (b) are the time nodes of increasing heat flux.

### 3.3.3. Effects of the Vertical Mixing

Generally, a strong wind could enhance oceanic mixing, which brings cold water from the lower layer to the surface and cools the upper layer [33]. Here, the wind speed is used to represent the potential vertical mixing. As shown in Figure 9a, the wind speed reduces by 0.6 m/s in most of the EKB in June, while increasing by 0.3 m/s in the northern EKB area. In Figure 9b, the wind speed in July is weaker than the climatological mean in the EKB area with a decrease of 1.8 m/s. On the contrary, wind speed strengthens and shows a positive anomaly of 1.2 m/s in the EKB area in August, with strong northwestern streamflow along the northern coast (Figure 9c). Generally, the weak sea surface wind could result in weak upper ocean mixing. Therefore, the weakened wind in July of 2021 could lessen the mixing in the upper ocean, hindering the warm SST from being mixed with the subsurface cold water, which helps keep warming the SST in the EKB and thus helps the occurrence of the MHWs. More robust quantitative analysis requires accurate realistic numerical modeling of the EKB area.

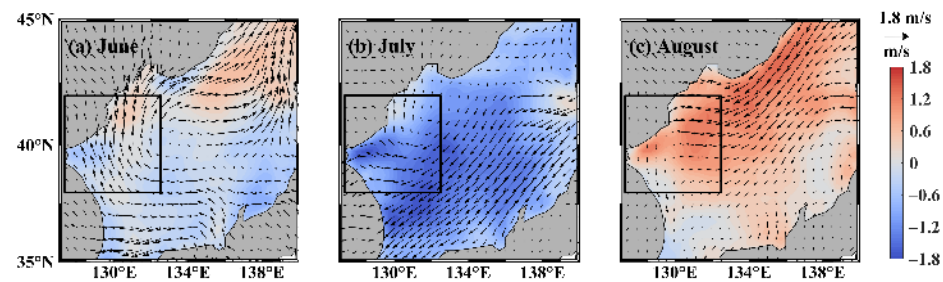


**Figure 9.** (a–c) 10-m wind speed anomaly (unit: m/s, vectors are the wind direction and the background color is the wind magnitude), from June to August 2021, relative to the climatology (1982–2021). The black box is the study area.

According to Figure 4, the metrics of MHWs in the summer of 2021 can be analyzed and roughly related to the spatial distributions of variables. A high value of Days and Frequency in the northern area in Figure 4a,b could be mainly associated with less total high net surface heat flux, owing to the strong blocking high in the northern of JES (Figure 6). Duration and three indices of intensity, however, are more pronounced in the central and southern of the EKB area, which may be due to lateral heat fluxes across the southern boundary and decreased sea surface wind from June to August 2021.

Based on the above analysis, the mechanisms for the occurrences of the summer 2021 MHWs are mainly caused by the atmospheric high-pressure system moving to the EKB area resulting in stronger shortwave radiation in the upper ocean. Other reasons provide a condition for less water cooling: the net positive lateral heat fluxes across open boundaries, and the weak sea surface wind over the EKB area. The combination of the above three factors introduces the occurrences of the summer MHWs in the EKB in 2021.

#### 4. Discussion

As discussed in Section 3, the general reasons for heat flux increase in the upper ocean involve heat fluxes across lateral boundaries, the sea surface, and the bottom level. The primary one is the heat fluxes across the sea surface associated with atmospheric forcing, similar to the conclusions of Kuroda and Setou [17]. However, there are other possible reasons, such as mesoscale eddies, that could cause the local SST increase. In this section, we discuss the effects of mesoscale eddies and the potential ecological impacts of MHWs.

##### 4.1. Effects of Mesoscale Eddies

Anticyclone (cyclonic) eddies usually have warm (cold) cores [34,35] and can be denoted by negative (positive) relative vorticity. Sea surface geostrophic current anomalies derived from satellite altimetry data (see data description in Section 2) are used to demonstrate that anticyclonic eddies are well presented in the EKB during the period when the MHWs take place in the summer of 2021 (1st July to 31 August 2021). Figure 10 shows eight snapshots of sea surface geostrophic current anomalies and the relative vorticities as examples. These strong anticyclonic eddies with warm cores can make contributions to warm the SST and keep the MHW for longer. The location of the anticyclonic eddies may be one of the reasons that high-intensity MHW events occur in the central and southern EKB area (Figure 4).

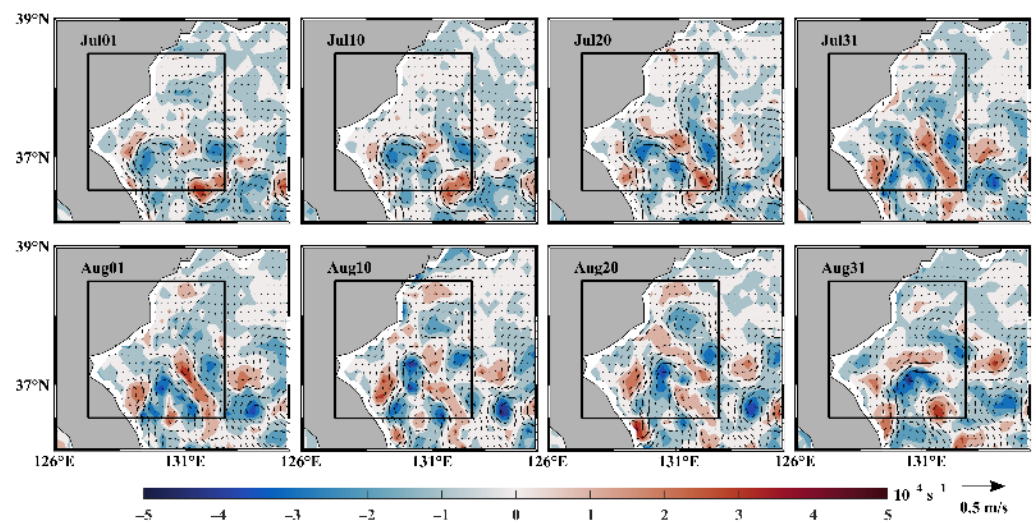


**Figure 10.** Sea surface geostrophic velocity anomalies (arrows, units: m/s) and related relative vorticities (color, units:  $s^{-1}$ ) from 1st July to 31 August 2021. The black box is the study area.

#### 4.2. Potential Ecological Impacts

There are very active biological processes in the JES, which are abundant in plankton and aquatic resources. However, Joo et al. [36] find that from 2003 to 2012, the annual primary output of the JES decreased by 13% every 10 years. It is speculated that one of the reasons is the shallower mixed layer, leading to extreme warming in the condition of the same solar radiation. The increasing SST may cause damage to the ecological environment.

In Figure 11, we analyze the 8-day mean CHL anomaly from July 20th to August 4th, 2021, the most severe period relative to the climatology (1997–2021). Since July 20th, the western part of the JES witnesses significant CHL decreases with a maximum of  $1 \text{ mg/m}^3$ . It can be seen clearly that biological processes indicated by CHL actually reduce the EKB, especially in coastal areas. The MHW occurrences may have a notable impact on the marine ecosystem and ecological benefits in the EKB, affecting aquatic revenues and the survival of marine species.

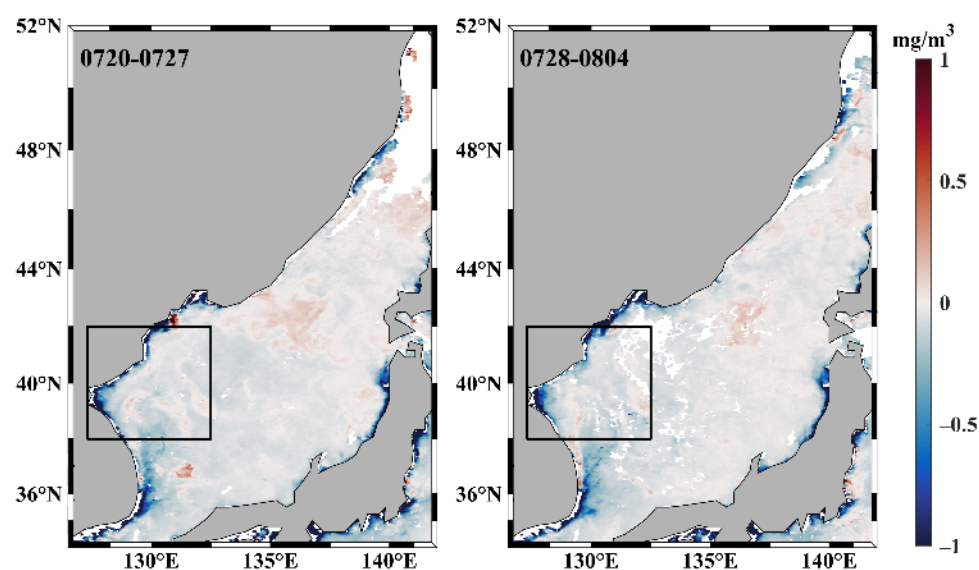


**Figure 11.** CHL anomaly (color shading, units:  $\text{mg/m}^3$ ) from 20th July to 4th August 2021, relative to the climatology (1997–2021). The black box is the study area.



## 5. Conclusions

This study analyzes the spatial distribution of MHWs in the JES from 1982 to 2021, focusing on the spatial and temporal distribution of MHWs in the EKB and its adjacent areas, and the single-point MHW event in the summer of 2021. Based on the climatology from June to August between 1982 and 2021, we discuss and explore the origin of MHWs in the EKB area from June to August 2021. The main conclusions are summarized as follows:

- (1) From 1982 to 2021, except for the Frequency, other MHW indices occur strongly in the western and central JES, especially in the EKB area, with rapidly increasing trends ( $p < 0.01$ ).
- (2) Severe MHW events in the EKB take place in the summer of 2021. A high Days spot (50–70 days) can be observed in the northern part of the EKB, and MeanInt reaches more than 4.5 °C in the southern EKB area. The total days and mean intensity of MHWs that occur in the EKB are 1.84 and 1.47 times more than those averaged in the JES, respectively.
- (3) The mechanisms for the occurrence of the MHWs in the summer of 2021 are primarily caused by the atmospheric high-pressure system moving to the EKB area resulting in strong solar radiation into the upper ocean and positive net heat flux. Other two reasons provide a condition for less water cooling: the net positive lateral heat fluxes across open boundaries, and the weak sea surface wind over the EKB area. The combination of the above three factors introduces the occurrences of the summer MHWs in the EKB in 2021.

Other possible reasons which cause the summer MHW events in 2021 could be relative to the impact of subpolar fronts, the semi-enclosed topography [20], and the increasing trend of 0.1 Sv per decade of the warm water transport across the Korea Strait as discussed in the literature [37], which need the oceanic numerical models to further investigate the issue.

**Author Contributions:** Conceptualization, C.D.; methodology, Y.Y.; validation, Y.F.; formal analysis, Y.Z.; writing—original draft preparation, S.C.; writing—review and editing, K.T.L.K.S.; funding acquisition, C.X. All authors have read and agreed to the published version of the manuscript.

**Funding:** This study was supported by the National Natural Science Foundation of China (42192562).

**Data Availability Statement:** The OISST v2.1 can be obtained at <https://www.ncei.noaa.gov/products/satellite-oceanography>, accessed on 27 March 2022. ERA5 is downloaded from <https://cds.climate.copernicus.eu/cdsapp#!/dataset/reanalysis-era5-single-levels-monthly-means?tab=form>, accessed on 8 November 2022. AVISO can be acquired at <https://cds.climate.copernicus.eu/cdsapp#!/dataset/satellite-sea-level-global?tab=form>, accessed on 30 July 2022. GHRSSST is from [https://data.remss.com/SST/daily/mw\\_ir/v05.0/netcdf/](https://data.remss.com/SST/daily/mw_ir/v05.0/netcdf/). Globcolour can be obtained from <https://hermes.acri.fr>, accessed on 29 November 2022.

**Acknowledgments:** The authors thank Brandon J. Bethel and Hui Gao for their kind help in this work.

**Conflicts of Interest:** The authors declare no conflict of interest.

## References

1. Cheng, L.; Trenberth, K.E.; Fasullo, J.; Boyer, T.; Abraham, J.; Zhu, J. Improved estimates of ocean heat content from 1960 to 2015. *Sci. Adv.* **2017**, *3*, e1601545. [CrossRef] [PubMed]
2. Cheng, L.; Abraham, J.; Trenberth, K.E.; Fasullo, J.; Boyer, T.; Locarnini, R.; Zhang, B.; Yu, F.; Wan, L.; Chen, X.; et al. Upper Ocean Temperatures Hit Record High in 2020. *Adv. Atmos. Sci.* **2021**, *38*, 1–8. [CrossRef]
3. Pörtner, H.-O.; Roberts, D.C.; Masson-Delmotte, V.; Zhai, P.; Tignor, M.; Poloczanska, E.; Weyer, N. *IPCC Special Report on the Ocean and Cryosphere in a Changing Climate*; IPCC Intergovernmental Panel on Climate Change: Geneva, Switzerland, 2019; p. 1.
4. Pearce, A.; Lenanton, R.C.; Jackson, G.; Moore, J.; Feng, M.; Gaughan, D.J. The “marine heat wave” off Western Australia during the summer of 2010/11. *Fish. Res. Rep.* **2011**, 222.
5. Hobday, A.J.; Alexander, L.V.; Perkins, S.E.; Smale, D.A.; Straub, S.C.; Oliver, E.C.; Benthuyssen, J.A.; Burrows, M.T.; Donat, M.G.; Feng, M.; et al. A hierarchical approach to defining marine heatwaves. *Prog. Oceanogr.* **2016**, *141*, 227–238. [CrossRef]

6. Oliver, E.C.J.; Donat, M.G.; Burrows, M.T.; Moore, P.J.; Smale, D.A.; Alexander, L.V.; Benthuisen, J.A.; Feng, M.; Sen Gupta, A.; Hobday, A.J.; et al. Longer and more frequent marine heatwaves over the past century. *Nat. Commun.* **2018**, *9*, 1324. [\[CrossRef\]](#) [\[PubMed\]](#)
7. Holbrook, N.J.; Gupta, A.S.; Oliver, E.C.; Hobday, A.J.; Benthuisen, J.A.; Scannell, H.A.; Smale, D.A.; Wernberg, T. Keeping pace with marine heatwaves. *Nat. Rev. Earth Environ.* **2020**, *1*, 482–493. [\[CrossRef\]](#)
8. Oliver, E.C.; Benthuisen, J.A.; Darmaraki, S.; Donat, M.G.; Hobday, A.J.; Holbrook, N.J.; Schlegel, R.W.; Gupta, A.S. Marine heatwaves. *Annu. Rev. Mar. Sci.* **2020**, *13*. [\[CrossRef\]](#)
9. Frölicher, T.L.; Fischer, E.M.; Gruber, N. Marine heatwaves under global warming. *Nature* **2018**, *560*, 360–364. [\[CrossRef\]](#)
10. Oliver, E.C.; Burrows, M.T.; Donat, M.G.; Sen Gupta, A.; Alexander, L.V.; Perkins-Kirkpatrick, S.E.; Benthuisen, J.A.; Hobday, A.J.; Holbrook, N.J.; Moore, P.J. Projected marine heatwaves in the 21st century and the potential for ecological impact. *Front. Mar. Sci.* **2019**, *6*, 734. [\[CrossRef\]](#)
11. Holbrook, N.J.; Scannell, H.A.; Gupta, A.S.; Benthuisen, J.A.; Feng, M.; Oliver, E.C.; Alexander, L.V.; Burrows, M.T.; Donat, M.G.; Hobday, A.J.; et al. A global assessment of marine heatwaves and their drivers. *Nat. Commun.* **2019**, *10*, 2624. [\[CrossRef\]](#)
12. Bond, N.A.; Cronin, M.F.; Freeland, H.; Mantua, N. Causes and impacts of the 2014 warm anomaly in the NE Pacific. *Geophys. Res. Lett.* **2015**, *42*, 3414–3420. [\[CrossRef\]](#)
13. Rodrigues, R.R.; Taschetto, A.S.; Sen Gupta, A.; Foltz, G.R. Common cause for severe droughts in South America and marine heatwaves in the South Atlantic. *Nat. Geosci.* **2019**, *12*, 620–626. [\[CrossRef\]](#)
14. Amaya, D.J.; Alexander, M.A.; Capotondi, A.; Deser, C.; Karnauskas, K.B.; Miller, A.J.; Mantua, N.J. Are long-term changes in mixed layer depth influencing North Pacific marine heatwaves? *Bull. Am. Meteorol. Soc.* **2021**, *102*, S59–S66. [\[CrossRef\]](#)
15. Feng, M.; Mcphaden, M.J.; Xie, S.; Hafner, J. La Niña forces unprecedented Leeuwin Current warming in 2011. *Sci. Rep.* **2013**, *3*, 1277. [\[CrossRef\]](#) [\[PubMed\]](#)
16. Gao, G.; Marin, M.; Feng, M.; Ding, Y.; Song, D. Drivers of Marine Heatwaves in the East China Sea and the South Yellow Sea in Three Consecutive Summers During 2016–2018. *J. Geophys. Res. Ocean.* **2020**, *125*, e2020JC016518. [\[CrossRef\]](#)
17. Kuroda, H.; Setou, T. Extensive Marine Heatwaves at the Sea Surface in the Northwestern Pacific Ocean in Summer 2021. *Remote Sens.* **2021**, *13*, 3989. [\[CrossRef\]](#)
18. Yao, Y.; Wang, J.; Yin, J.; Zou, X. Marine heatwaves in China’s marginal seas and adjacent offshore waters: Past, Present, and Future. *J. Geophys. Res. Ocean.* **2020**, *125*, e2019JC015801. [\[CrossRef\]](#)
19. Wang, D.; Xu, T.; Fang, G.; Jiang, S.; Wang, G.; Wei, Z.; Wang, Y. Characteristics of Marine Heatwaves in the Japan/East Sea. *Remote Sens.* **2022**, *14*, 936. [\[CrossRef\]](#)
20. Wang, H.; Chen, S.; Wang, N.; Yu, P.; Yang, X.; Wang, Y.; Zhang, Y. Evaluation of multi-model current data in the East/Japan Sea. In Proceedings of the 2020 3rd IEEE International Conference on Information Communication and Signal Processing (ICICSP 2020), Shanghai, China, 12–15 December 2020; pp. 486–491.
21. Cai, R.; Tan, H.; Kontoyiannis, H. Robust surface warming in offshore China seas and its relationship to the east Asian monsoon wind field and ocean forcing on interdecadal time scales. *J. Clim.* **2017**, *30*, 8987–9005. [\[CrossRef\]](#)
22. Huang, B.; Liu, C.; Banzon, V.; Freeman, E.; Graham, G.; Hankins, B.; Smith, T.; Zhang, H.-M. Improvements of the Daily Optimum Interpolation Sea Surface Temperature (DOISST) Version 2.1. *J. Clim.* **2020**, *34*, 2923–2939. [\[CrossRef\]](#)
23. Chelton, D.B.; Schlax, M.G.; Samelson, R.M.; de Szoeke, R.A. Global observations of large oceanic eddies. *Geophys. Res. Lett.* **2007**, *34*, L15606. [\[CrossRef\]](#)
24. Chelton, D.B.; Schlax, M.G.; Samelson, R.M. Global observations of nonlinear mesoscale eddies. *Prog. Oceanogr.* **2011**, *91*, 167–216. [\[CrossRef\]](#)
25. Oliver, E.; Benthuisen, J.; Bindoff, N.; Hobday, A.J.; Holbrook, N.J.; Mundy, C.N.; Perkins-Kirkpatrick, S.E. The unprecedented 2015/16 Tasman Sea marine heatwave. *Nat. Commun.* **2017**, *8*, 16101. [\[CrossRef\]](#) [\[PubMed\]](#)
26. Zhao, Z.; Marin, M. A MATLAB toolbox to detect and analyze marine heatwaves. *J. Open Source Softw.* **2019**, *4*, 1124. [\[CrossRef\]](#)
27. Yao, Y.; Wang, C. Variations in summer marine heatwaves in the South China Sea. *J. Geophys. Res. Ocean.* **2021**, *126*, e2021JC017792. [\[CrossRef\]](#)
28. Zhao, N.; Manda, A.; Han, Z. Frontogenesis and frontolysis of the subpolar front in the surface mixed layer of the Japan Sea. *J. Geophys. Res. Ocean.* **2014**, *119*, 1498–1509. [\[CrossRef\]](#)
29. Black, E.; Blackburn, M.; Harrison, G.; Hoskins, B.; Methven, J. Factors contributing to the summer 2003 European heatwave. *Weather* **2004**, *59*, 217–223. [\[CrossRef\]](#)
30. Lee, T.; Hobbs, W.R.; Willis, J.K.; Halkides, D.; Fukumori, I.; Armstrong, E.M.; Hayashi, A.K.; Liu, W.T.; Patzert, W.; Wang, O. Record warming in the South Pacific and western Antarctica associated with the strong central-Pacific El Niño in 2009–10. *Geophys. Res. Lett.* **2010**, *37*, L19704. [\[CrossRef\]](#)
31. Choi, W.; Bang, M.; Joh, Y.; Ham, Y.-G.; Kang, N.; Jang, C.J. Characteristics and Mechanisms of Marine Heatwaves in the East Asian Marginal Seas: Regional and Seasonal Differences. *Remote Sens.* **2022**, *14*, 3522. [\[CrossRef\]](#)
32. Feng, Y.; Bethel, B.J.; Dong, C.; Zhao, H.; Yao, Y.; Yu, Y. Marine heatwave events near Weizhou island, beibu gulf in 2020 and their possible relations to coral bleaching. *Sci. Total Environ.* **2022**, *823*, 153–414. [\[CrossRef\]](#) [\[PubMed\]](#)
33. Shin, H.; Lee, J.; Kim, C.; Yoon, J.H.; Hirose, N.; Takikawa, T.; Cho, K. Long-term variation in volume transport of the Tsushima warm current estimated from ADCP current measurement and sea level differences in the Korea/Tsushima Strait. *J. Mar. Syst.* **2022**, *232*, 103750. [\[CrossRef\]](#)

34. Ansorge, I.J.; Jackson, J.M.; Reid, K.; Durgadoo, J.V.; Swart, S.; Eberenz, S. Evidence of a southward eddy corridor in the South-West Indian ocean. *Deep. Sea Res. Part II Top. Stud. Oceanogr.* **2015**, *119*, 69–76. [[CrossRef](#)]
35. Dong, C.M.; McWilliams, J.C.; Liu, Y.; Chen, D. Global heat and salt transports by eddy movement. *Nat. Commun.* **2014**, *5*, 1–6. [[CrossRef](#)] [[PubMed](#)]
36. Joo, H.T.; Park, J.W.; Son, S.H.; Noh, J.H.; Jeong, J.Y.; Kwak, J.H.; Saux-Picart, S.; Choi, J.H.; Kang, C.K.; Lee, S.H. Long-term annual primary production in the Ulleung Basin as a biological hot spot in the East/Japan Sea. *J. Geophys. Res. Ocean.* **2014**, *119*, 3002–3011. [[CrossRef](#)]
37. Kida, S.; Takayama, K.; Sasaki, Y.N.; Matsuura, H.; Hirose, N. Increasing trend in Japan Sea Throughflow transport. *J. Oceanogr.* **2020**, *77*, 145–153. [[CrossRef](#)]

**Disclaimer/Publisher’s Note:** The statements, opinions and data contained in all publications are solely those of the individual author(s) and contributor(s) and not of MDPI and/or the editor(s). MDPI and/or the editor(s) disclaim responsibility for any injury to people or property resulting from any ideas, methods, instructions or products referred to in the content.